CHALMERS

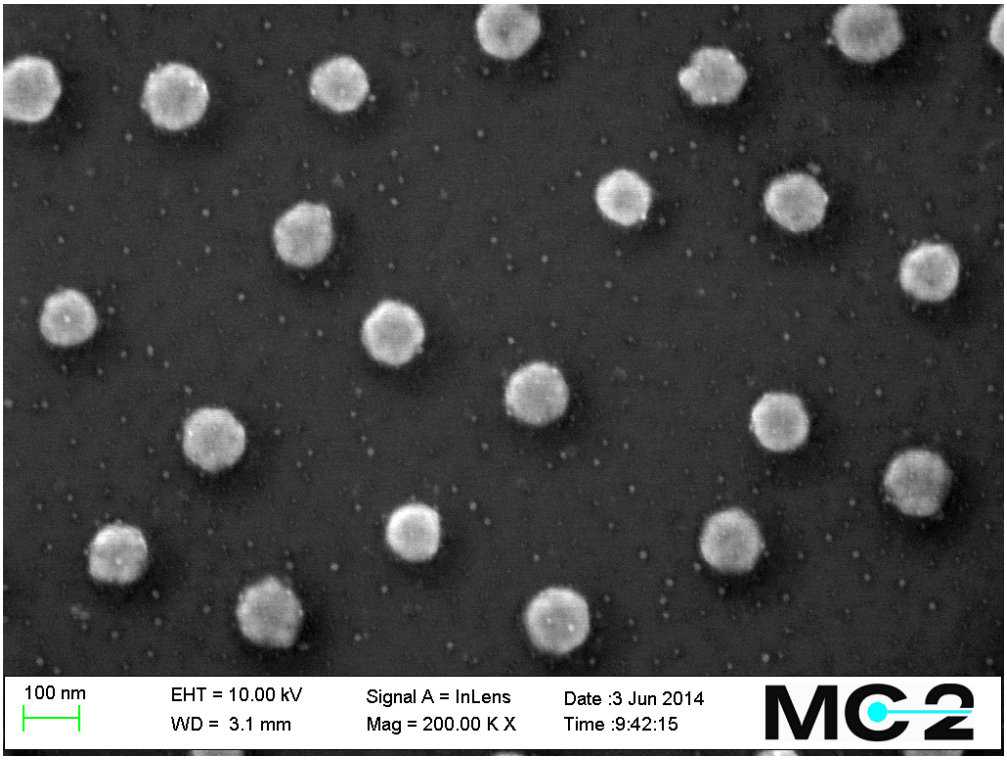

Towards Plasmon-Enhanced Heterogeneous Catalysis on Metal Nanoparticles

Master of Science Thesis in Applied Physics

JENNY ANDERSSON

Department of Applied Physics
Division of Chemical Physics
Chalmers University of Technology
Gothenburg, Sweden 2014

Thesis for the degree of Master of Science in Engineering Physics

Towards Plasmon-Enhanced Heterogeneous Catalysis on Metal Nanoparticles

Jenny Andersson

Department of Applied Physics
Division of Chemical Physics
Chalmers University of Technology
Gothenburg, Sweden 2014

Towards Plasmon-Enhanced Heterogeneous Catalysis on Metal Nanoparticles
JENNY ANDERSSON

Department of Applied Physics
Division of Chemical Physics
SE-412 96 Gothenburg, Sweden
Telephone +46(0)31-772 10 00

Cover illustration: *SEM picture depicting the dispersed nanoantennas on the sample surface.*

Printed by: Chalmers Reproservice Göteborg, Sweden 2014

Towards Plasmon-Enhanced Heterogeneous Catalysis on Metal Nanoparticles

Jenny Andersson
Department of Applied Physics
Division of Chemical Physics
Chalmers University of Technology
Gothenburg, Sweden 2014

Abstract

Heterogeneous catalysis is a vital part of the chemical industry. The energy efficiency is, for many processes, somewhat less than desired. The main reason for this is high operating temperatures due to activation barriers. Research has shown that catalysts which also are plasmonically active yield higher reaction rates under illumination. It is theorised that hot electrons originating from the decay of plasmonic resonances assist in molecular dissociation via transient electron attachment. In reactions where dissociation is associated with the rate-limiting step, this could enhance the reaction rate at constant temperature. Plasmonic structures are characterised by build-ups in electric field intensity in the vicinity of the structure, as well as elevated absorption efficiencies ($Q_{abs} > 1$). Due to the low energy efficiencies of catalytic reactions, it is of interest to utilise plasmonic nanostructures to aquire new reaction pathways. A structure with a Au plasmonic nanoantenna, above which Pt catalytic particles are deposited, is proposed. The electric field surrounding the Au nanoantenna would induce a polarisation in the catalytic particle, and hence, enhance the energetic charge carrier creation via locally enhanced absorption. The proposed structure is created using hole-mask colloidal lithography together with physical evaporation techniques. An experimental assembly is designed to test the structures. A significant increase in catalytic rate is observed under illumination of the sample, however, the effect is not conclusively determined to be connected to the plasmonic nanoantennas since it is also observed during illumination of only the catalyst itself. This implies a direct optical excitation in the catalyst nanoparticle as the reason for the observed enhancement.

Keywords: Heterogeneous catalysis, LSPR, hydrogen oxidation, HCL

Acknowledgements

First and foremost, I would like to thank my examiner and supervisors.
Christoph Langhammer, for the opportunity to perform this thesis, theory discussions and guidance throughout the work.
Carl Wadell, for experimental guidance, ideas, discussions, troubleshooting and consequently answering to emails within a few minutes.
Svetlana Syrenova, for clear and concise instructions in sample fabrication, characterisation and cleanroom attire application.

Adam Arvidsson, for endless discussions about theory, layout, graph colours, the weather and any and all other topics.

Kristina Wettergren and the rest of the **Chemical physics group** for interest and input into the project.

Pascal Gebauer and **William Hallberg** for feedback on the project and the report.

Jenny Andersson, Göteborg, 2014-06-05

Contents

1

Introduction

Commercial heterogeneous catalysis, today, is associated with high operating temperatures and significant noble metal content. These are in turn related to certain drawbacks, the former with compromised long term stability and energy efficiency, and the latter with high cost. Unfortunately, these constituents are essential due to the high activation barriers associated with the rate-limiting step in many commercially important catalytic reactions. Obviously, these aspects have a deleterious effect on the overall energy efficiency of the reaction. Hence, it is of interest to decrease the supplied thermal energy into the reaction by, for example, providing an alternative reaction pathway. This thesis aims at the exploration of hot electron based reaction pathways in heterogeneous catalysis via the incorporation of plasmonic nanostructures.

1.1 Background

With the energy efficiency decrease associated with high operating temperatures, room temperature solutions are highly sought after. A lowering in operating temperature, however, introduces the need for an alternative route over the activation barrier. Previous research[1, 2, 3] have found an increase in the catalytic reaction rate for illuminated samples where the nanosized catalytic particles also exhibit plasmonic resonances. The increase is significant and raises the question of whether this is industrially applicable.

It has been theorised that this effect is driven by hot-electron transfer arising from the decay of the plasmonic resonance, where the electron creates a transient ion state at the reacting species in the catalytic reaction. The transient state facilitates the dissociation segment of the reaction and, where dissociation is the rate-limiting step, augments the entire reaction rate.[1, 2, 3] This could allow

for utilisation of even low intensity light sources, such as sunlight, to enhance a heterogeneous catalytic reaction on a metal catalyst.

1.1.1 Heterogeneous Catalysis

Heterogeneous catalysis refers to the branch of catalysis where the reacting and the catalytic species are in different thermodynamic phases. Most common, as well as the one implemented in the thesis, is the case of solid metal catalyst and gas phase reactants. The solid catalytic particles can be either supported or unsupported. The renowned example of heterogeneous catalysis, emission control in vehicles, regards supported catalysis. That is, the catalytic particles are dispersed over a supporting mesoporous (porous material with a pore size of 2 - 50 nm) substrate, typically an oxide. This yields a very high specific surface area, allowing for a large quantity of catalytic particles in a small volume. Supported heterogeneous catalysis is common in many other areas as well, such as industrial and vehicle emission control, and will be the considered instance of catalysis for this thesis.

1.1.2 Plasmonic Resonances

The typical catalytic particles do not to any great extent absorb photons in the visible spectral range. Plasmonic nanoparticles with larger absorption cross-sections do, however, absorb photons efficiently and are able to transfer some of the absorbed energy in different forms to an adjacent catalytic particle. For example, via an effective polarisation of the catalytic particle, which gives rise to enhanced absorption. A plasmonic nanoparticle is able to sustain plasmon resonances, and different metals perform with varying results in this aspect. Particularly strong resonances in the natural light spectral range are found in the metals Au, Ag and Cu.[4] The resonant frequency depends primarily on a set of four factors: electron density, effective electron mass together with the size and shape of the electron distribution.[5]

The type of plasmonic resonances occurring at the surface of a material, at the interface between a metal and a dielectric, is referred to as a surface plasmon, which is somewhat different from a bulk plasmon. When the resonances occur in a nanometer sized particle, the electron cloud experiences the effects of boundaries, and is referred to as a localised surface plasmon. For a comprehension of the concept of a surface plasmon, the resonance can be visualised as a coherent, collective oscillation of the electron cloud against the fixed positive ion cores. The occurrence of plasmonic resonances gives rise to striking optical properties and absorption efficiencies. The latter being one of the main reasons for their applicability. Plasmonic nanostructures exhibit absorption efficiencies larger than unity ($Q_{abs} > 1$), that is, they absorb more photons than what is geometrically impinging on their cross sectional area.[6] In connection to this elevated efficiency,

an enhancement in the electrical field in the vicinity of the plasmonic particle is present. The enhancement is remarkable, up to several orders of magnitude.[5]

With the somewhat extraordinary absorption features of these plasmonic nanoparticles, one would like to utilise the absorbed energy in order to enhance a catalytic reaction. The near-field enhancement can be utilised for efficient polarisation of an adjacent particle.[7] For a catalytically active particle, this polarisation may intensify the energetic electron-hole pair generation, leading to an enhancement in the catalytic reaction rate.

1.2 Purpose/Aim

The project aims at demonstrating that localised surface plasmon resonance via the incorporation of small catalytically active nanoparticles can be used to enhance the reaction rate by hot-electron transfer to empty (LUMO) orbitals of the adsorbate molecule associated with the rate-limiting step.

1.2.1 Scope

This thesis is experimental in nature and the focus will not be to determine the underlying mechanisms from a theoretical basis. Experiments will mainly focus on the oxidation reaction of hydrogen over a Pt catalyst. For the plasmonic structure, Au nanodiscs will be used. The choice of materials can gradually be extended to include other catalyst or plasmonic particle arrangements.

1.2.2 Research Focus

One of the fundamental questions regarding this thesis is whether or not the observed effect is due to an electron transfer as a result of the plasmonic de-excitation. The previously observed results could be attributed to the inherent temperature increase during illumination. Therefore, the main purpose of this thesis is to determine whether the effect is plasmonic in nature and which parameters are most relevant.

1.3 Method

In order to test the hypothesis, samples containing a base of plasmonic Au nanostructures must be created. This is performed via hole-mask colloidal lithography. Directly in contact with the nanostructures, a support layer of Al_2O_3 will be deposited. The catalytic Pt particles will then be evaporated on top. In Figure 1.1, a qualitative description of the proposed structure can be seen.

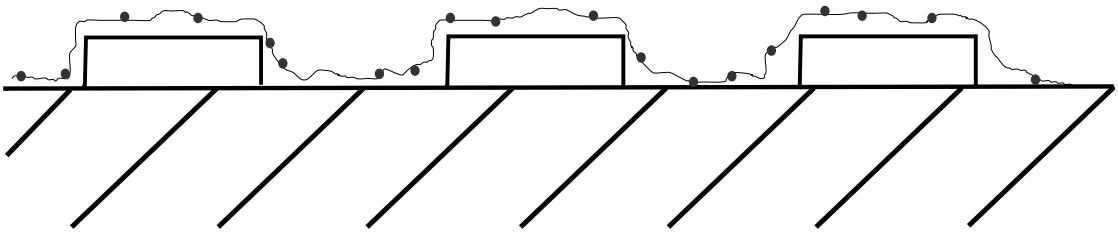

Figure 1.1: Qualitative illustration of the proposed concept. The illustration is of a vertical cross section, where the Au nanodiscs can be seen in cross section on top of a glass substarate. The mesoporos Al_2O_3 covers the nanodiscs and provides support for the smaller, Pt, catalytical particles.

1.4 Outline

The reader will be taken through the thesis, starting with a brief theory description. First an introduction to the concepts of nanoplasmonics and heterogeneous catalysis is given after which a description of used techniques and materials together with the practical experimental set-up is presented. After completion of the theory chapters, the results will be presented followed by a discussion section and conclusions.

2

Plasmonic Resonances

NANOPLASMONICS IS THE branch of optical condensed matter science which deals with nanoscaled optical phenomenon in metal systems.[8] The most remarkable feature in the nanoplasmonic field is the intense enhancement in the electric field intensity in the surroundings of the plasmonic nanoparticles. This enhancement, together with the large absorption efficiencies of plasmonic nanstructures, is the foundation of many nanoplasmonic applications.

2.1 Bulk Plasmon

The concept of a plasmon is possible to comprehend even within the frames of classical physics. Since the plasmon primarily is an instance of conductors, the Drude model[9] can be used for a hint into the origin of the quasiparticle, the plasmon. For this, the dielectric function for a metal is needed.[10]

$$\epsilon = 1 - \frac{\omega_p^2}{\omega + i\gamma\omega}$$

Here, γ corresponds to the damping of the electromagnetic wave in the metal. First, one should notice that the existence of a plasmon is directly dependant on that the real part of the dielectric function, ϵ, is negative. Since the electric field inside a metal obeys the wave equation, it should satisfy:

$$-\nabla^2\mathbf{E} = \frac{\omega^2}{c^2}\epsilon(w)\mathbf{E}$$

For a real, positive dielectric function, the solutions become oscillatory, hence, radiation propagates through the material. For a real, negative dielectric function however, the solutions will be exponentially decaying in the material, hence, the

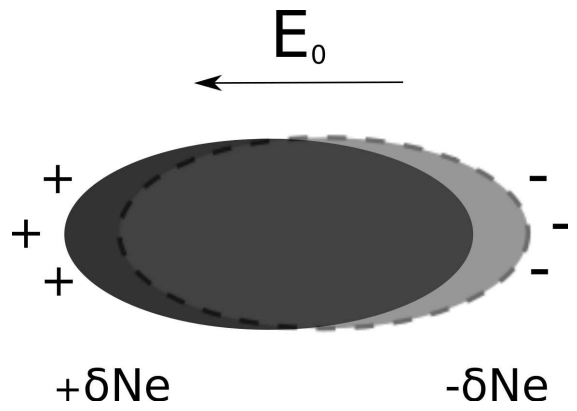

Figure 2.1: An incident electromagnetic field causes a displacement of the charge distribution. At resonant frequencies, the charge distribution forms an oscillatory motion.

radiation will be absorbed. It is not strictly necessary for the dielectric function to be entirely real, a satisfying criterion is that $\mathrm{Im}\,\epsilon << -\mathrm{Re}\,\epsilon$.[8] It is, from simple mechanics, possible to derive the plasma frequency, ω_p, for a free electron gas, such as would be found in a metal.[6]

$$\omega_p^2 = \frac{Ne^2}{m_e \epsilon_0}$$

In the given expression for the plasma frequency, N is the density of free electrons and m_e is the effective mass of an electron. For the simplicity of the calculations, a collision free electron gas is assumed. This means that in equilibrium the number density of both positive ions and electrons are constant, N. If the electrons are somewhat displaced, from for example an impinging electrical field, the resulting non-uniform charge distribution will then be the origin of an electric field (Figure 2.1).

This electric field will act to restore the equilibrium charge distribution. The electrons, however, will acquire a momentum from the restoring force and overshoot their equilibrium positions. Hence, an oscillatory motion is in place. Denoting the electron distribution out of equilibrium with δN yields the electric field according to:

$$\nabla \cdot \mathbf{E} = \frac{e\delta N}{\epsilon_0}$$

Given that the displacement of the electrons is slight, $|\delta N/N| << 1$, the equation of continuity can be approximated according to:

$$\nabla \cdot \mathbf{u} = \frac{\partial}{\partial t}\frac{\delta N}{N}$$

These are all under the assumption of a free electron gas, where $\mathbf{u}$ is the velocity field of this gas. Neglecting magnetic and pressure forces, which for the purpose will be adequate assumptions, the equation of motion for the electron gas can be found.

$$\frac{\partial \mathbf{u}}{\partial t} + (\mathbf{u} \cdot \nabla)\mathbf{u} = -\frac{e}{m}\mathbf{E}$$

This expression can be simplified further by recognising that the first term will be in the order of U/τ and the second term, U^2/L where U, τ and L are characteristic quantities with the units of m/s, 1/s and m. Using appropriate values of these quantities yields $1/\tau >> U/L$, therefore, the expression for the equation of motion can be simplified to:

$$\frac{\partial \mathbf{u}}{\partial t} = -\frac{e}{m}\mathbf{E}$$

With the use of some vector identities an expression for the charge distribution displacement is obtained.

$$\frac{\partial^2}{\partial t^2}\frac{\delta N}{N} + \omega_p^2 \frac{\delta N}{N} = 0$$

By definition, the solutions to this equation should be in plane wave form, that is:

$$\mathbf{E} = \mathbf{E_0} e^{i\mathbf{k}\cdot\mathbf{r} - i\omega t}$$
$$\frac{\delta N}{N} = C_0 e^{i\mathbf{k}\cdot\mathbf{r} - i\omega t}$$

By insertion of these into the previously yielded expressions, two requirements for the solutions emerges.

$$i\mathbf{k} \cdot \mathbf{E} = \frac{e\delta N}{\epsilon_0}$$
$$C_0(\omega_p^2 - \omega^2) = 0$$

For this set of equations, there are two solutions. The first requires that $C_0 = 0$ which implies that $\mathbf{k} \cdot \mathbf{E} = 0$, meaning that the plane wave solution is transverse. For the second solution, $\omega_p^2 = \omega^2$. Neglecting the damping in the expression for the dielectric function, this corresponds to $\epsilon(\omega_p) = 0$. The meaning of the zero value dielectric function can be found from Maxwells equations.[11]

$$\nabla \cdot \epsilon \mathbf{E} = \rho$$
$$\nabla \cdot \mathbf{B} = 0$$
$$\nabla \times \mathbf{E} = -\frac{\partial \mathbf{B}}{\partial t}$$
$$\nabla \times \mathbf{H} = \mathbf{J} + \frac{\partial \epsilon \mathbf{E}}{\partial t}$$

The second and fourth of these statements, given a zero free current, together with $\epsilon(\omega_p) = 0$ yields $\mathbf{B} = 0$. Consequently, $\nabla \times \mathbf{E} = 0$, hence, the electric field is longitudinal. This somewhat lengthy argument results in the description of the bulk plasmon as a longitudinal oscillation in the electron density. The quasiparticle description of the plasmon, which arises from the quantisation of these plasma oscillations, contains the energy $\hbar\omega_p$.[6]

2.2 Localised Surface Plasmon

Now that the concept of a plasmon is firmly set, the question of what happens when the electron cloud no longer can be considered infinite arises. The arranging forces in the bulk plasmon are generated by Coulomb interactions between electrons and positive ions. This is a long range interaction and it stands to reason that in a small system, the effects of boundaries should become apparent.

In small particles absorption effects not apparent in their parent bulk material can, not only be visible, but also dominate the absorption and scattering spectra. In these nanoscale systems, electromagnetic surface modes are responsible for the elevated absorption features.

These surface modes are of a somewhat difficult origin to understand. For a theoretical background to this, the problem is to solve Maxwells equations for the electric field inside the particulate and the surrounding dielectric medium. The problematic section of this would be the interface between particle and medium, where the dielectric function is discontinuous. It can be shown that a satisfying criteria for this is energy conservation, which can be satisfied by keeping the tangential component of the electric field continuous over the boundary.[6] If one were to endeavour such a task, it is suggested to do so for the case of a spherical particle for which an analytical solution is possible.

In a spherical symmetry, the equations can be split up in separate equations for the radial distance, polar and azimuthal angles. After that, it is simply a matter of assuming a separable solution. Doing this, one would arrive at the radial part being spanned by the spherical Bessel functions, Legendre functions for the polar angle and simple trigonometric functions for the azimuthal angle. The total solution can hence be expressed in the form of vector spherical harmonics.[6]

With the analytical expression for the electric field at the nanoparticle, scattering and absorption cross sections can be constructed. And now, with a bit of algebra the cross sections can be calculated in the limit $x \to 0$, that is, vanishingly small particles. At this, a set of complex frequencies for which the scattering coefficient is infinite can be found, but due to the complexity of the frequencies the corresponding modes are said to be virtual. There are, however, real frequencies close to the complex ones for which there will be a resonance in the cross sections. Such frequencies are associated with normal modes, termed surface modes. These surface modes are what are generally intended with the term localised surface plasmon resonance.

In similarity with the bulk plasmons, which have the energy $\hbar\omega_p$, there are surface plasmons in thin films with the energy $\hbar\omega_p/\sqrt{2}$ and the surface plasmons discussed previously, the sphere, with energy $\hbar\omega_p/\sqrt{3}$.[6] Following the previous discussion of the electromagnetic surface modes as the reason for the elevated absorption in small particles, clearly there can also be surface phonons, given the excitation of the crystal lattice instead of the electron cloud. Infrared surface modes are often referred to as surface phonons. Expanding this somewhat more, a surface polariton is just a surface mode with no restriction to the size of the sphere.

Since nature does not consist of perfectly shaped spheres in vacuum, it is of interest to theoretically study non-uniform particles. In the spherical particles, a plenitude of surface modes can be excited. However, in non-uniform particles, the dipole mode dominates strongly and higher order modes are severely quenched.[5] This allows for the use of quasistatic theory, for particles smaller than the wavelength of the impinging light. This will, however, not be discussed.

2.2.1 Absorption and Scattering

It has previously been discussed that plasmonic metallic nanostructures couple especially well to incident resonant photons via the excitation of electromagnetic surface modes. It is established that the surface plasmons depend on that the real part of the dielectric function, ϵ, for the plasmonic material is negative. These plasmons are particularly distinct as resonances when the losses are small enough, that is, $\operatorname{Im}\epsilon << -\operatorname{Re}\epsilon$.[8] These two criteria are what determines whether a metal is a good plasmonic material or not. With these properties together with high absorption in the dominate natural light frequencies, the most common plasmonic materials Au, Ag and Cu are found.[4]

One of the most prominent features of the plasmonic nanoparticles is their ability to have absorption and scattering efficiencies larger than unity. These efficiencies are defined accordingly:

$$Q_{abs} = \frac{C_{abs}}{A}$$
$$Q_{sca} = \frac{C_{sca}}{A}$$

Here, C denominates the absorption/scattering cross section and A denotes the cross sectional area perpendicular to the incident beam. Having these efficiencies larger than unity corresponds to the absorption of more light than what is geometrically incident upon them. To understand this, Bohren and Huffman[6] invokes the electromagnetic concept of the Poynting vector. The Poynting vector represents the directional energy flux density in the electromagnetic field. Without the existence of a particle in the electric field, the Poynting vector would simply be a vector parallel to the propagation of the incident photon flux. The field lines of the Poynting vector can be seen in Figure 2.2. In a similar way as the introduction of particle into an electric field changes those field lines, the introduction of a plasmonic nanoparticle changes the energy flux field lines, giving rise to the abnormally large absorption and efficiencies larger than unity.

2.2.2 Near-field Enhancement

Surface plasmon resonances are characterised by an intense build-up of electric field intensity in the vicinity of the nanostructure. The enhancement can be derived from the quality factor of the plasmonic metal.[8] This quality factor yields the amplification of the near-field compared to the external field and is given by:

$$Q = \frac{\omega}{2 \cdot \tau} \tag{2.1}$$

Here, ω is given by the surface plasmon frequency and τ is the relaxation rate which in turn is dependent on the dielectric function for the metal. The field enhancement is proportional to a factor Q^2 and ranges for noble metals from 10^2 to 10^4.[12]

In between plasmonic structures, the field intensity can reach particularly high intensities. These locals are referred to as hot-spots.[4] The distinct enhancement arises from the multiplication of quality factors for different nanoparticles together with constructive interference and enhancement due to different geometrical structures.[12] Deleterious for many applications, however, the enhancement is reduced due to radiative losses in larger nanopaticles.

2.3 Decay Modes

The excited plasmonic resonances have two possible decay modes. The first, radiative decay via the emission of a photon, second, non-radiative decay. The radiative

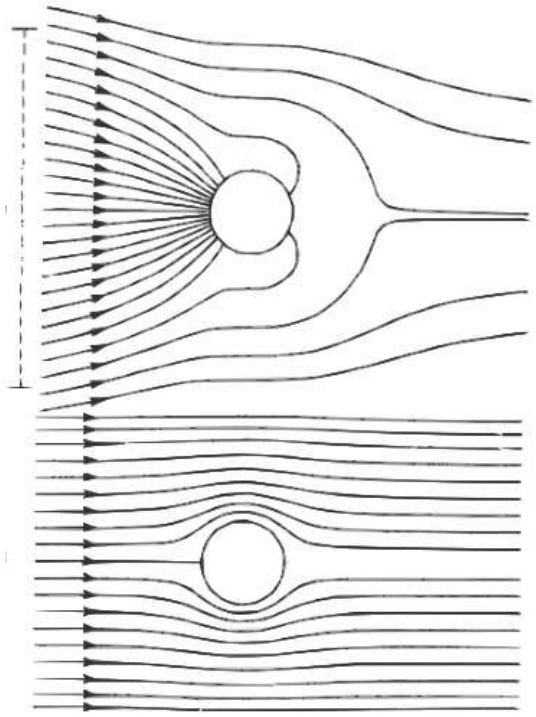

Figure 2.2: Illustration of the origin of absorption and scattering efficiencies larger than unity. The graph demonstrates the effect on the field lines of the Poynting vector caused by illuminating a plasmonic nanoparticle. Top figure depicts the effect of an excited localised surface plasmon in a particle under illumination. Figure reprinted with permission from [6]. Copyright (2014) John Wiley and Sons.

rate is proportional to the number of conduction electrons in the system.[8] In the second decay mode, the absorbed energy is transferred into a single electron-hole pair. Given enough energy, this electron is termed a hot-electron, that is, an electron with enough energy to traverse a potential barrier. If not given enough energy, the electron will thermalise and cause an increase in the local temperature. The first decay mode is predominantly present in larger nanostructures while the second dominates in smaller structures.

2.4 Plasmonic Antenna

With a second metallic particle in the vicinity of the larger plasmonic nanoparticle the enhanced electric field in the vicinity will induce a polarisation in the adjacent particle. For the purpose of this thesis, the second particle will be a catalyst. This polarisation may then enhance the energetic charge carrier creation in the catalytic particle, via enhanced photon absorption, leading to an increase in charge carrier

injection into adsorbates.[7] In a sense, the plasmonic structure would work as a ”funnel” for the energy into the catalyst. However, there could be a second effect from the charge carrier generation. Hot electrons coupling to lattice phonons could transform the plasmonic structure into a localised heat source, yielding an increase in catalytic activity, a thermal effect.

3

Heterogeneous catalysis

Catalysis is a vital part of the chemical industry. It is essential for it to evolve and to be economical. Much of the large scale manufacturing of chemical compounds relies on catalysis, either to make reactions happen at all or fast enough, or to achieve economic vindication. Heterogeneous catalysis can, in most cases, be described as surface reactions on metal particles. These reactions can be split up into three different steps. The first is adsorption, the second is dissociation and the last is desorption from the surface.

3.1 Catalysis

The basics of a catalytic reaction is that a catalyst accelerates the reaction without being consumed in the process. The catalyst offers an alternative, lower energy, route over the activation barrier. Although the catalysed reaction path may be more complex, the lower activation costs makes the alternative path energetically favourable. However, even though the activation energy is lower with a catalyst, the overall free energy change is the same for the catalysed reaction as for the uncatalysed. A schematic picture over the catalysed reaction can be seen in Figure 3.1.

Heterogeneous catalysis is the term intending the types of catalysis where the catalyst and the reactants are in different thermodynamic phases. Most commonly, the case of a solid catalyst and gas phase reactants. In this type of catalysis, the reacting species are associated with active sites at the catalyst surface. At these sites, the catalyst forms bonds to the reactants allowing the reaction to take place in the adsorbed state.[13] The catalytic cycle can be represented by the following equations:

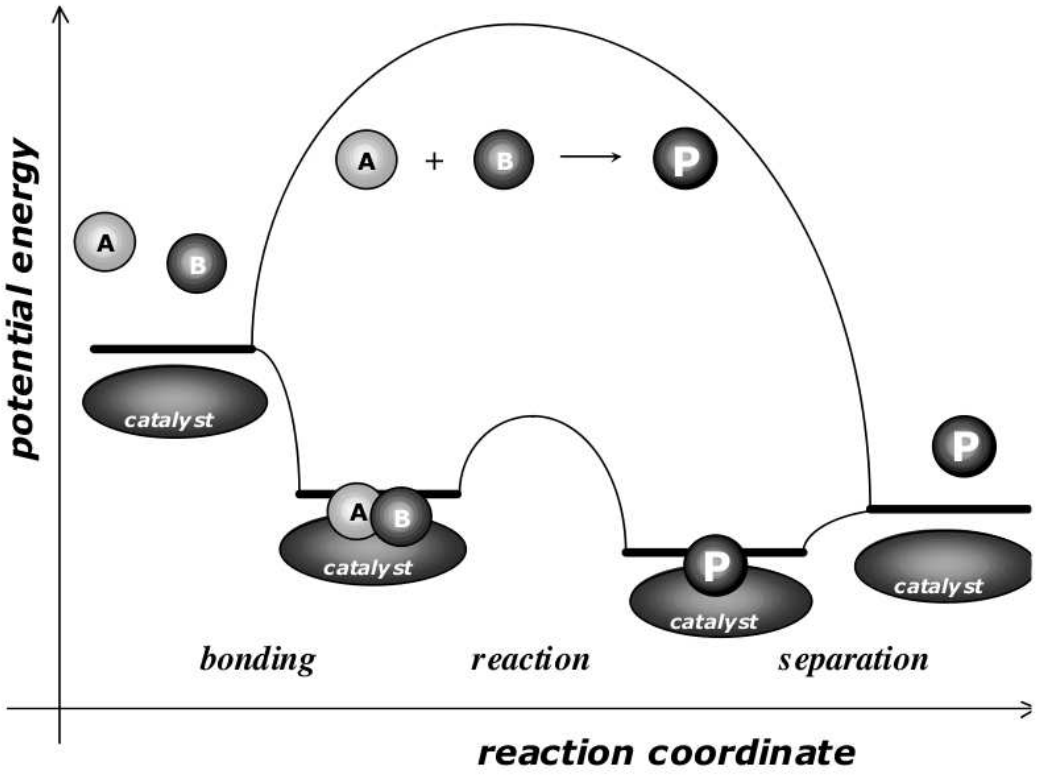

Figure 3.1: A schematic view over the catalytic cycle. The starting reactants and the end product is the same, no matter the reaction path. The catalysed path contains more reaction steps than the uncatalysed, regardless, the lower activation energy makes it energetically favourable. Figure reprinted with permission from [13]. Copyright (2014) John Wiley and Sons.

$$\mathrm{R} + * \underset{k_1^-}{\overset{k_1^+}{\rightleftarrows}} \mathrm{R}^*$$

$$\mathrm{R}^* \xrightarrow{k_2^*} \mathrm{P} + *$$

Here, R represents the reacting species and * represents the active site. When the intermediate R^* is formed it has a probability for moving along the reaction coordinate to form the product species or to revert back, into the reacting species. For a second order reaction, that is, two reacting species, the intermediates must be located on adjacent active sites for the reaction to move along the reaction coordinate. Each active site can only be associated with one single species at a time, leading to the microscopic concept of turnover frequency. The turnover frequency is defined as the number of molecules converted per active site and

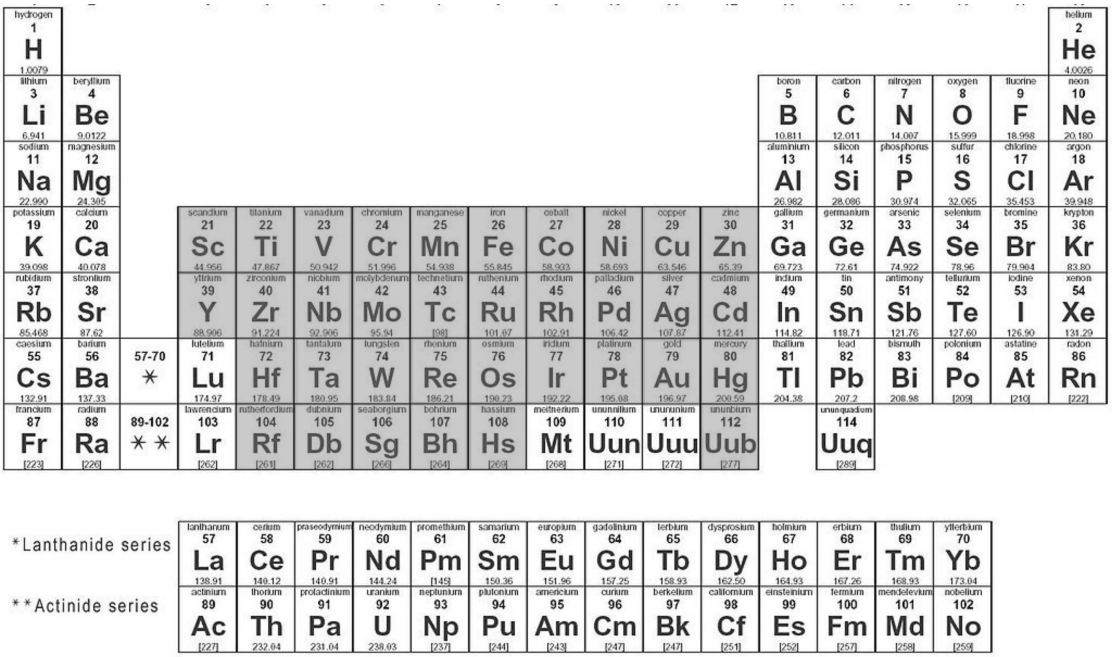

Figure 3.2: Transition metals are present amongst the d-block elements in the periodic table. Their unfilled d-orbitals is the underlying reason for their catalytic applicability.

unit time. At low temperatures, the reaction is kinetically hindered by the micro kinetics at the particle surface.

3.2 Transition Metals

Transition metals (Figure 3.2) are most often used as catalyst. The density of states for a transition metals contains, in addition to their broad *sp*-band, also d electrons. The main reason for their catalytic applicability is the presence of incompletely filled d-orbitals.[13] These partly filled d-orbitals work qualitatively as both electron donors and acceptors.

3.2.1 Adsorption

There are two types of adsorption which the reactants can experience on the metal surface. A molecule approaching the metal experiences a potential landscape. In order to form a complex with the surface, the molecule must undergo an inelastic collision. The loss of energy allows for the molecule to get trapped in a surface-molecule potential well. The first local minimum in the potential landscape constitutes the first type of adsorption, physisorption. Physisorption constitutes a Van der Waals type bond with the surface. That is, a weak bond and the species easily

desorb via thermal vibrations from the surface.

From a more significant overlap in the electronic wavefunctions for the surface and the molecule, the second type of adsorption arises, chemisorption. The broad *sp*-band of the transition metal interacts with the molecular orbitals, causing a lowering in energy. The same type of interaction occurs between the *d*-orbitals and the molecule, here, the result is a splitting into bonding and anti-bonding orbitals.

Since the energy levels have been lowered, Fermi electrons from the metal may partially fill the anti-bonding orbitals of the molecule. The filling of these orbitals results in a stronger bonding between the surface and molecule, however, it also results in a weakening of the intra-molecular bonds. This is the founding of molecular dissociation on metal surfaces.

In the important case of a second order reaction, the two reacting species compete for the same active sites. In this type of competitive adsorption, the stronger binding species will dominate with respect to surface coverage. In many cases, the stronger binding species constitutes a poisoning effect for the entire reaction. This, since both reactants must be adsorbed to the surface for the reaction to proceed.

3.2.2 Dissociation

Sufficient filling of an anti-bonding orbital for the molecule to dissociate may occur in a transition state. That is, reaction proceeds via an activated complex, the transition state, for which the metal donates an electron. This state is located on top of the reaction energy barrier along the reaction coordinate. A transition to the activated complex can also occur via collision with a molecule, or, via the hot electrons arising from the decay of a plasmonic resonance.[3] The electron is transferred to the lowest unoccupied molecular orbital (LUMO), which, due to the orbital shift is an anti-bonding orbital. A transition negative ion state is created. The bond length for this transition state at equilibrium is elongated compared to the original state. Hence, when the transition state relaxes, the species end up in an excited state which then can pass the reaction barrier.

3.3 Product Formation

There are two main reaction mechanisms for which the reactants can transform into the product species. Langmuir-Hinshelwood mechanism and Eley-Rideal mechanism. In the Langmuir-Hinshelwood model, both reactants are adsorbed to the surface and hence react in the chemisorbed phase. The Eley-Rideal model assumes that one of the reactant species is adsorbed to the surface and the other is in gas phase reacting with the chemisorbed species. In heterogeneous catalysis, Langmuir-Hinshelwood is the most common mechanism.[13]

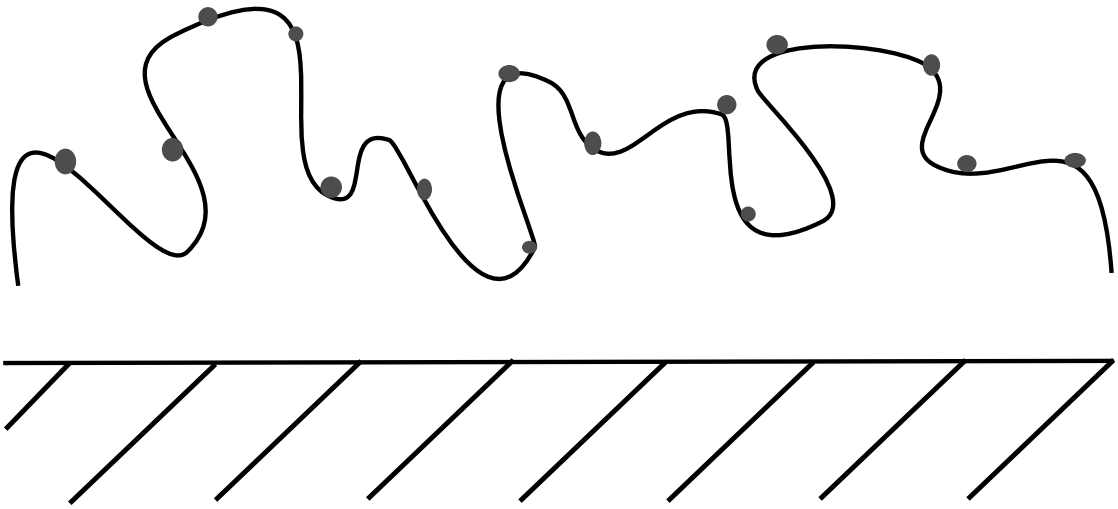

Figure 3.3: Small catalytic particles supported on a porous substrate.

3.4 Reaction Dynamics

Certain stable reactant species cause a large release of energy during the chemisorption reaction. These species are not reactive and do not desorb from the catalyst. Hence, they prevent further adsorption by the catalyst. This effect is known as catalyst poisoning. For sufficiently high temperatures, the poisoning species will desorb. The chemisorption strength varies for different metals, in general, the absorption strength is at large in the left of the transition period and decreases moving to the right over the period.

The turnover frequency is easily increased via an increase in temperature. In the area of chemical reaction mechanisms the reaction rate has an exponential dependence.[13] This is given by the Arrhenius equation.

$$K(T) = \nu e^{E_a/RT}$$

Here, E_a represents the activation energy. The reaction rate is, however, dominated by the micro kinetics only over a certain temperature interval. At a transition temperature, the rate limiting factor for the reaction will be the mass transport in the surface layer closest to the catalyst, hence, the reaction speed will only increase to a certain temperature where it levels off.

The catalyst can be either supported or unsupported. For supported catalysts, a carrier material with a large surface area, such as a mesoporous structure, is used as the support on which the catalysts is deposited (Figure 3.3). In the case of unsupported catalyst, the entire catalytic structure consists of the same, catalytic, material. For their great importance, as well as for practical reasons, the case of supported heterogeneous catalysis is studied.

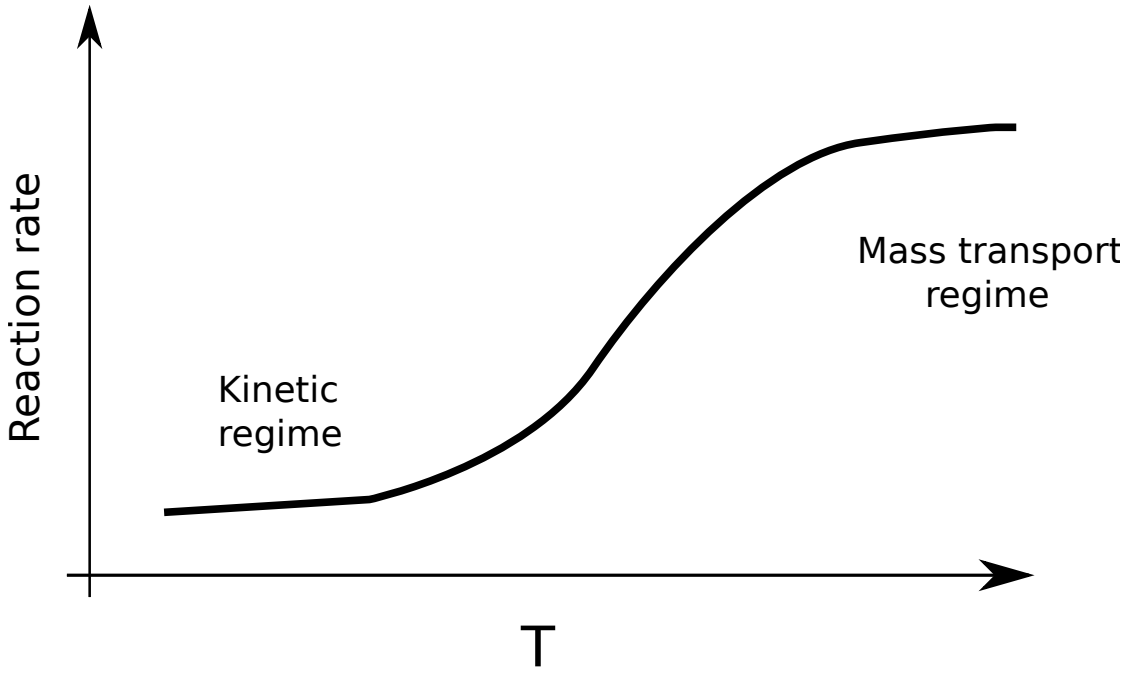

Figure 3.4: Schematic illustration of the catalytic reaction rate. At low temperatures, the rate is limited by the micro kinetics on the particle surface. At higher temperatures, the reaction rate is hindered by the limited diffusion close to the particles.

The porous structure of the substrate layer adds extra steps for the catalytic reaction. Before the adsorption of reactants at the active sites can take place, the reactants must diffuse through the boundary gas layer at the catalysts surface. Most of the catalytic particles will be dispersed in the mesopouros network, hence, the reactants must also diffuse through the support material to reach the catalytic active sites. The same diffusive steps also must occur after the catalytic reaction. The characteristics behaviour of a general catalytic reaction rate can be seen in Figure 3.4

3.5 Hydrogen Oxidation

In this work, the studied reaction is the oxidation reaction of H_2 into H_2O over a Pt catalyst. This reaction is given according to:

$$H_2 + \frac{1}{2}O_2 \rightarrow H_2O$$

In a simplified and somewhat ideal case, the Pt particles will relax to their stable form, the so called Wulff shape. The surface area of this particle consists of two different surfaces, the (111) and the (211) surface. Reactants adsorbed to

active sites on these different surfaces have distinctly different potential barriers to traverse for the reaction steps to occur. In the extension of this, the rate-limiting step is hard to determine as it depends on the present surfaces at the catalytic particles. For this simplified case, the reaction steps based on DFT[14] simulations can be seen in Figure 3.5.

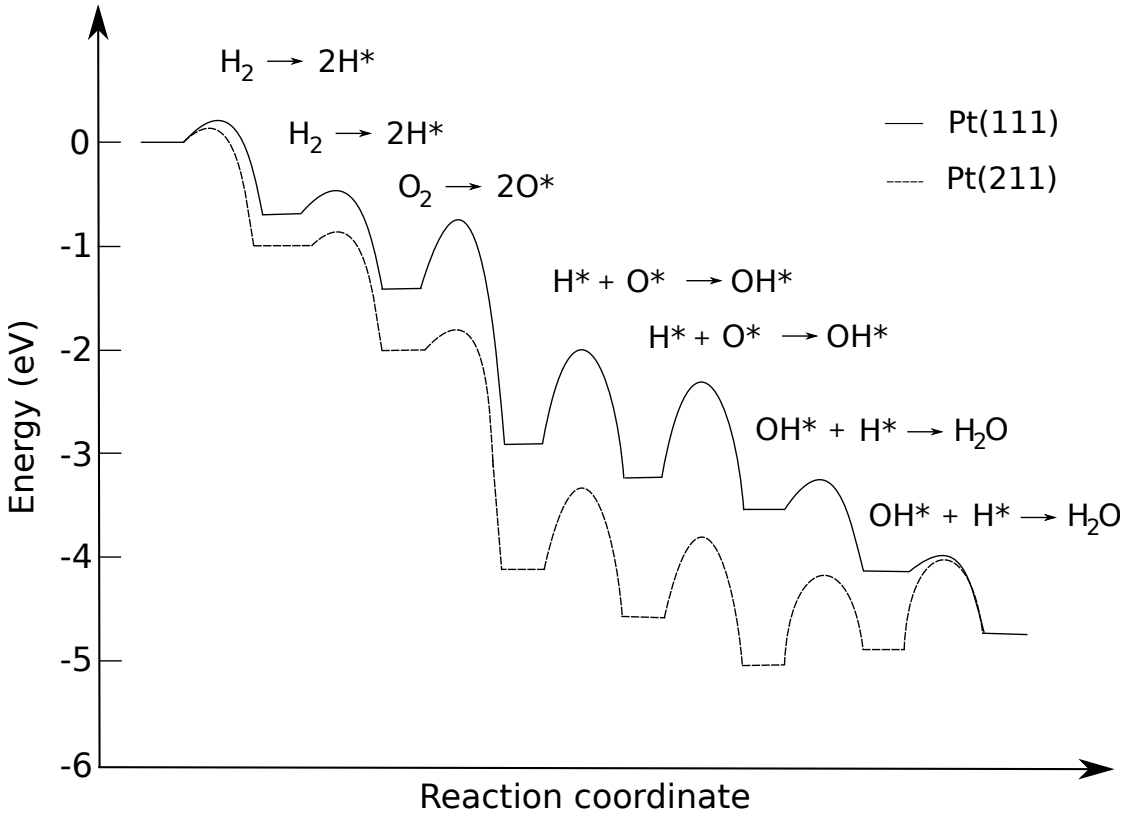

Figure 3.5: The reaction landscape for H_2 combustion reaction over a Pt catalyst. The different lines correspond to adsorption on different surfaces, the (111) and the (211) surface. Figure based on DFT calculations performed by Anders Hellman.

From this, a high activation barrier can be observed for the dissociation of oxygen at the (111) surface. It has been shown, albeit for reaction occurring directly on the plasmonic particles surface, that hot electron generation from the decay of plasmonic resonances aid in dissociation processes. Both for oxygen[1] and for hydrogen[3]. Since electron transfer to LUMO orbitals is the basis for molecular dissociation, given that dissociation is a rate-limiting step, plasmonic excitation and decay should be able to enhance the reaction rate.

4

Methods and materials

Samples with plasmonic nanostructures were created using hole-mask colloidal lithography (HCL). Directly in contact with these nanoparticles, a support layer was sputtered. This layer constitutes the support for the catalytic particles, which were evaporated onto the surface. The fabricated samples were then placed in a reaction chamber with a gas inlet and a mass spectrometer attached to the outlet. The product gas composition was measured in real time, yielding the reaction rate.

4.1 Hole-mask Colloidal Lithography

HCL is a bottom-up method for fabrication of surface based nanostructures.[15] The method relies on the self assembly of polystyrene beads (PS) on a charged surface for the arrangement of nanostructures The materials were deposited on a substrate of borosilicate glass. A schematic view over the fabrication process can be seen in Figure 4.1

The first step in HCL is deposition of a sacrificial layer. For this purpose, PMMA was used. The sacrificial layer was spin-coated onto a substrate after which it was solidified at a hot plate. The sample was then briefly exposed to a oxygen plasma in order to decrease the hydrophobicity.

After deposition of the sacrificial layer, a charged polyelectrolyte should be added to the surface. This is followed by deposition of the polystyrene (PS) beads onto the substrate. The PS is in a colloidal suspension and are oppositely charged compared to the polyelectrolyte. The attraction between the PS and the surface together with the mutual repulsion between particles determines the arrangement of particles over the sample

Once the PS particles are dispersed on the sample, a thin-film, plasma etch

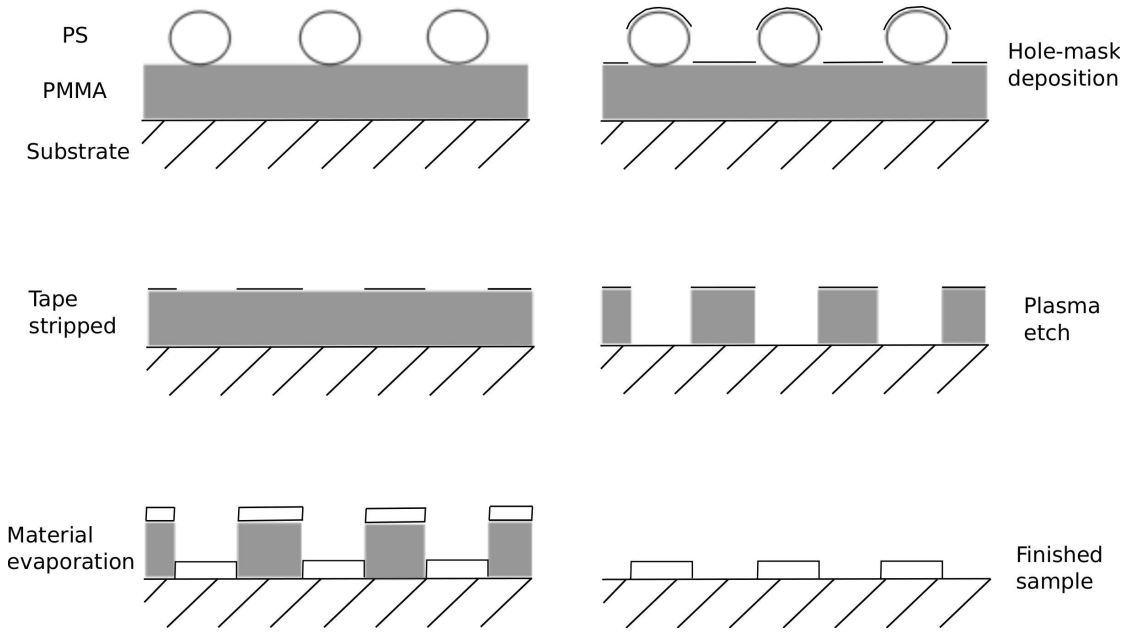

Figure 4.1: The figure depicts the essential steps in hole-mask colloidal lithography. The arrangement of the nanostructures corresponds to the dispersion of the PS beads, which is a self arrangement due to electrostatic forces. Once the mask is evaporated, it will be stripped leaving holes in the thin film. These holes expose the sacrificial PMMA layer underneath and cavities can be etched down to the substrate. The desired material is then evaporated and the remaining PMMA is dissolved

resistant, layer (Cr or Au) is evaporated (Lesker, PVD 225). This layer is what eventually turns into the hole-mask for which the method has gained its name. With the PS beads on the surface, applying tape allows for selective stripping of the mask. Hence, the PS beads translates into holes in the evaporated film, that is, the hole-mask.

The holes in the mask expose the sacrificial PMMA layer. The sample is then subjected to an oxygen plasma etch. The oxygen plasma etches away the exposed PMMA and creates cavities down to the substrate. With the substrate unprotected, the plasmonic metal can be evaporated onto the sample. The arrangement of the plasmonic structures will, therefore, match that of the PS beads.

After the desired plasmonic metal has been deposited, it covers the entire sample. In order to dispose of the unwanted material, the sample is put into acetone. The remaining PMMA will dissolve of the surface, taking the surplus material along. Left is the substrate with the desired plasmonic structure.

4.2 Materials for Nanofabrication

The used sacrificial layer was polymethyl methacrylate (PMMA), a common polymeric material. The used PMMA had a molecular weight of 950 000 g/mol and was spin-coated at 2000 rpm over the course of one minute. Afterwards, the PMMA was solidified at a hot plate for 10 min at 170° C. From these parameters the layer thickness can be determined to about 300 nm.

The diameter of the plasmonic nanoparticle discs are determined by the diameter of the polystyrene beads. The PS beads are suspended in a colloidal solution with 0.2 wt% PS. Particles with an average diameter ranging from 31 nm to 300 nm were used.

The used polyelectrolyte was a PDDA solution at 0.2 wt% in de-ionised water. The PDDA has a high positive charge density and will hence attract the negatively charged PS.

For the hole-mask, about 20 nm of Cr was used and the plasmonic antennas consisted of 30 nm of Au (evaporated in Lesker PVD 225). The support layer was made from about 8 nm of Al_2O_3 (sputtered in FHR MS150) and the catalytic particles were a few Ångstroms of Pt (evaporated in AVAC HVC600).

4.3 Sputter Deposition

Directly in contact with the plasmonic nanoparticles, the support layer for the catalyst was deposited. This was accomplished via sputter deposition. In the sputter deposition process, highly energetic particles impact on a target material. If the particles have a high enough energy, the target will eject material leading to a vapour deposition on the substrate. That is, the selected material will condense on the substrate forming a thin film.

4.4 Catalyst Deposition

The catalytic particles were dispersed over the support layer, above the nanoparticles. For this, a physical vapour technique, identical to that used for deposition of the thin-film hole-mask, was used. The desired material was evaporated in high vacuum under electron bombardment, leading to the condensation of a thin film on the sample. The samples were afterwards annealed, leading to agglomeration into particles.

4.5 Experimental Set-up

The reaction was performed in a vertically oriented reaction vessel (Harrick Scientific), which allowed for both illumination of the catalyst and temperature control

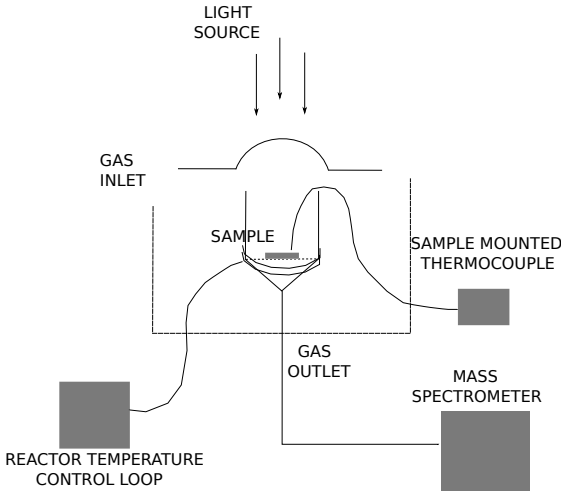

Figure 4.2: Schematic view over the experimental set-up. The samples were placed in a reaction chamber (Harrick Scientific) which was illuminated and temperature controlled.

of the surrounding chamber. The reactant gas is let in via a channel at the wall. At the bottom of the vessel, there is an outlet for the product gas. The sample is suspended above the base with a net. Reactant gas flow was controlled via mass flow controllers, which delivered a mixture of the gases, hydrogen, oxygen and argon. Attached at the outlet is the mass spectrometer. This gives in real time the constituents of the product gas. For a sketch of the experimental set-up, see Figure 4.2. The reaction chamber is equipped with a feedback-system for temperature control and measurement. An additional thermocouple was coupled directly into the chamber in contact with the sample surface, in order to estimate potential heat effects from the light source.

4.5.1 Mass Spectrometry

The outlet from the reaction chamber is subjected into the mass spectrometer (Pfeiffer Vacuum OMNIstar) via a differentially pumped and heated capillary tube, the gas is diluted by being pumped down in a vacuum chamber. The gas is ionised and the constituents are characterised via a mass filter which separates the molecules according to their charge-mass ratio.The ionisation process consists of the gases being bombarded with electrons, emitted from a heated cathode. The electrons are accelerated via an applied voltage between the anode and cathode. In the intermittent space between the electrodes the neutral gas molecules are present. Collision with the energised electrons yields single and multiple positive ions.

When the particles have left the mass filter, the ion current is measured using a secondary electron multiplier (SEM). The measured current is a function of the

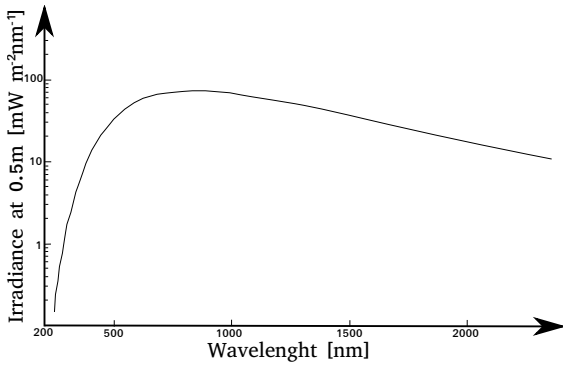

Figure 4.3: The irradiance spectrum for the light source. Maximum irradiance is found in the visible spectral range.

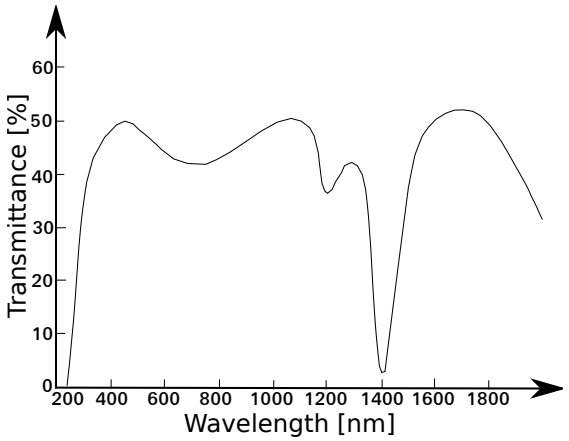

Figure 4.4: The transmittance for the fiber. Over the visible spectral range, the average transmittance is 45%.

partial pressure of the constituents in the inlet gas.

4.5.2 Light Source and Optical Fiber

The light source utilises a quartz tungsten halogen lamp (Oriel Instruments) mounted in a lamp housing (Oriel Instruments), which irradiates primarily in the visible spectral range. The total irradiance can be seen in Figure 4.3. The light was passed through an optical fiber bundle of fused silica (Oriel Instruments). When the light passes through the fibre, the irradiance is altered by the transmittance of the fiber bundle. The transmittance of the bundle is about 45% over the visible spectral range and can be seen in Figure 4.4.

5

Results

In the following chapter, the main results obtained during this thesis project are presented. Several different measurement series have been performed in order to establish the effect of illumination of the Pt catalysed H_2 oxidation reaction and the possible enhancement due to adjacent Au plasmonic nanoantennas or to light absorption directly in the Pt catalyst itself.

5.1 Particle Size and Distribution

The used nanoantennas were Au discs. Their average size, and the distribution over the sample surface, were confirmed using SEM. The dispersion for a typical sample with Au nanodiscs of an average diameter of about 100 nm can be seen in Figure 5.1.

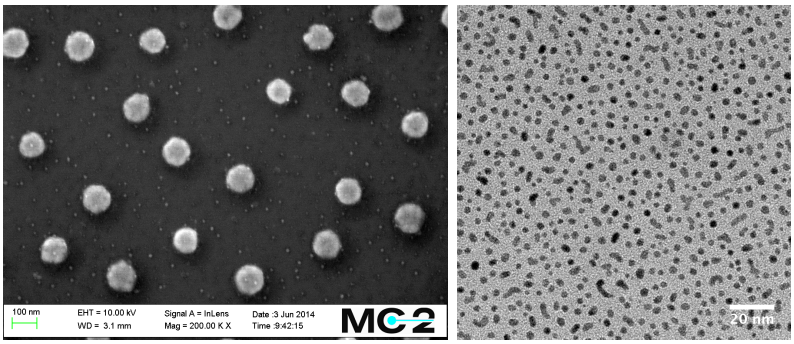

Figure 5.1: (Right) SEM picture over the Au nanoantennas. The antennas cover about 10% of the surface, and have an average diameter of 100 nm. (Left) TEM picture over dispersed Pt (5 Å), the resulting particle size is about 4 nm.

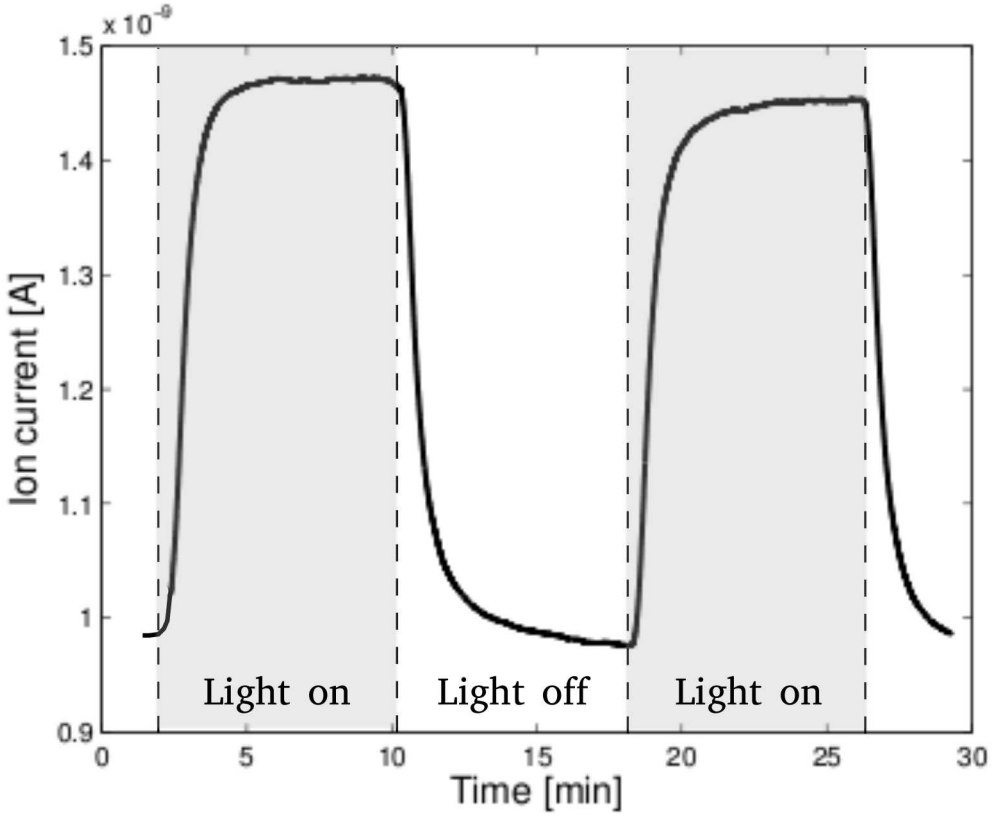

Figure 5.2: The response of the H_2O production rate to illumination. At reactor temperature $T_R = 175\,°C$ and set light source intensity of 250 W.

5.2 Au Nanoantennas

The fabricated samples were annealed at 300 °C for 22 hours. Then, the samples were placed in the reaction chamber and subjected to a gas flow of 225 ml/min, consisting mostly of Ar (carrier gas) together with equal parts H_2 and O_2 (0.6% each).

5.2.1 Illumination Response

The production of H_2O over a standard sample (Au nanodiscs with a disc diameter of 100 nm and a height of 30 nm covered with a support layer of 7 nm of Al_2O_3, with 6 Å Pt dispersed over the surface) was measured. After some time, a stable background was obtained. At this point, the sample was subjected to periodic illumination. The light source was on for 8 min, then off for another 8 min, repeatedly. The effect of the illumination of the samples can be seen in Figure 5.2. These results clearly indicate that the light has an effect on the production of H_2O. For

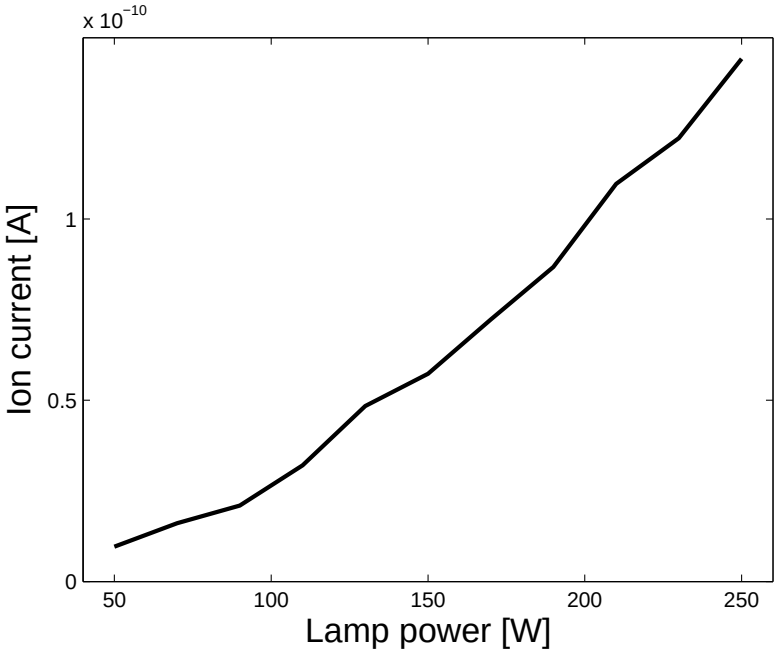

Figure 5.3: The difference in steady state ion current before illumination and after illumination at different intensities at $T_R = 175\,°C$. Intensity is given as the set-point for light source

the indicated test, the light source was set to 250 W.

The reaction increase, that is, the difference in ion current during steady state with the light on and off respectively, as a function of illumination intensity was measured. The measurement was performed at reaction chamber temperature, $T_R = 175\,°C$ and sample surface temperature $T_S = 120°$ C. The resulting difference as a function of intensity can be seen in Figure 5.3. The intensity is given as the set-point for the light source power output.

Similar tests were performed without a sample in the reactor. The light was periodically turned on and off at different reactor temperature set points (T_R from 50 °C to 220 °C). No effect on the mass spectrometer signal was found for temperature, nor illumination.

The time, from which the light was turned on at steady state to that the reaction reached a new steady state was considered the step time for the response. The dependence of this time to different parameters was investigated. As a first test, the effect of mass flow was measured in order to establish whether the response time was related to mass transport trough the reactor. The gas flow was set to different values (150 ml/min, 200 ml/min, 250 ml/min). For each, two reactant concentrations were tested (0.4%, 0.8%). Results from this measurement can be seen in Figure 5.4. No definite dependence on mass flow and concentration for the

step time is observed, which would have been expected for a diffusive property. The results would seen to indicated that there is a loss of information regarding the kinetics of the reaction when the gas is transported through the mass spectrometer capillary.

Secondly, the effect of temperature was measured. Reactor temperature was varied ($T_R = 215, 195, 150, 120, 90, 55\,^{\circ}C$). Results for the intermediate temperature range can be seen in Figure 5.5. A clear effect on step response from temperature is observed. The time for the increase to reach half maximum was calculated and can be seen in Figure 5.6. The clear temperature dependence is speculated to arise partly from the overall faster kinetics, partly from the characteristic behaviour of a catalytic reaction (Figure 3.4). At higher temperatures, a small increase in temperature yields a proportionate larger response compare to lower temperatures (the energy released from the exothermic reaction act to enhance the reaction further).

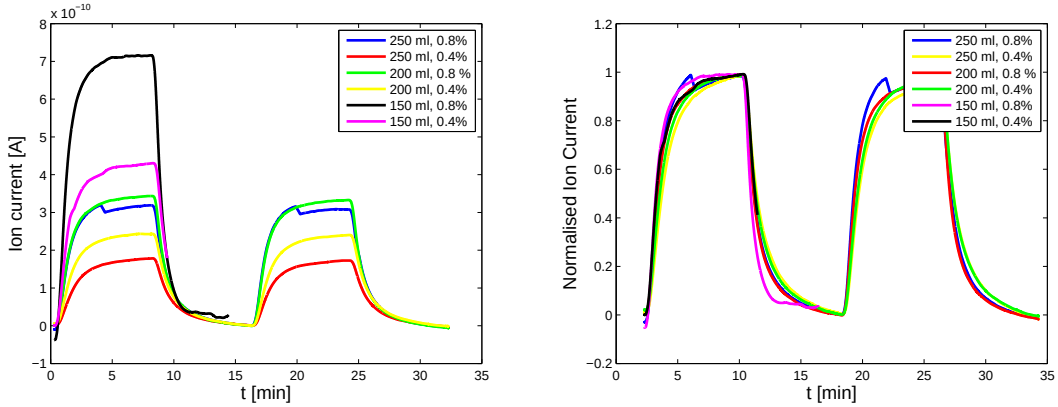

Figure 5.4: The step response was investigated for different reactant concentrations (0.4%, 0.8%) and gas flows (150 ml/min, 200 ml/min, 250 ml/min). (Left) The different amplitudes are displayed. Note that for the lower flows, only one step is included as for these flows, the mass spectrometer was not able to maintain a stable current. (Right) Values are given as a normalised ion current, after the highest value for each measurement. A moving average of a hundred data points was deployed for smoothing of the currents. The effect of gas flow and reactant concentration appears negligible.

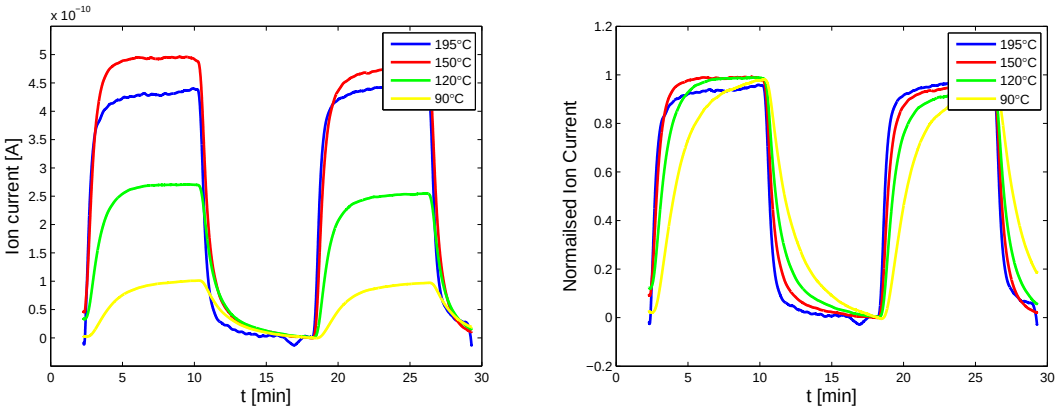

Figure 5.5: The step response was investigated for different reactor temperatures (depicted in graph, T_R =195, 150, 120, 90 $°C$). (Left) The different amplitudes for the different temperatures are displayed. (Right) Values are given as a normalised ion current, after the highest value for each measurement. A moving average of a hundred data points was deployed for smoothing of the currents. A clear effect on step response from temperature is observed.

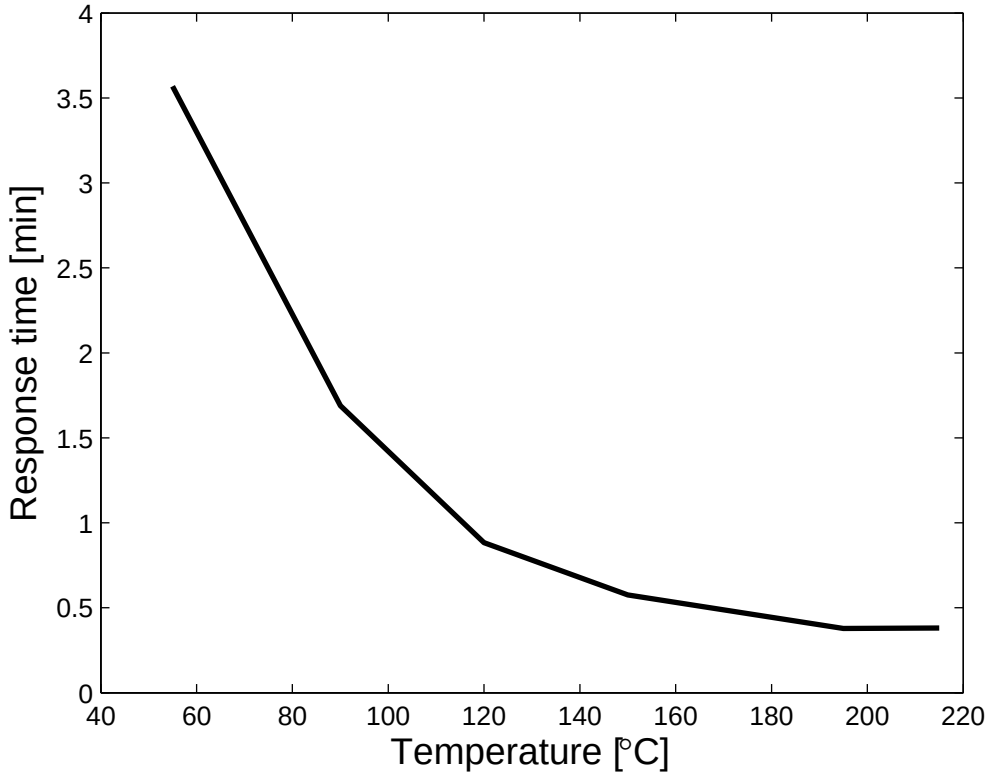

Figure 5.6: The time for the increase to reach half of its maximum value was calculated. Clearly, an increase in reactor temperature causes a decrease in response time after switching on the light.

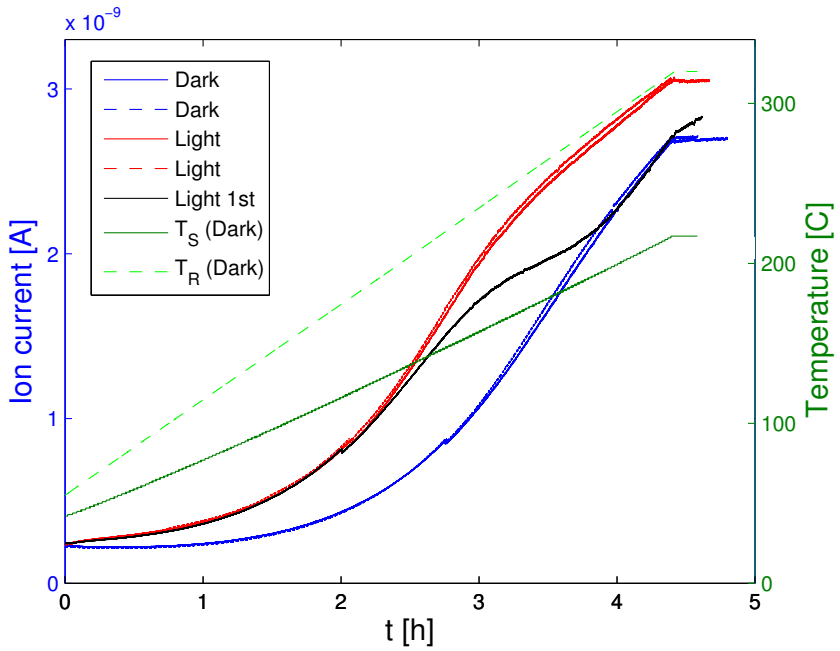

Figure 5.7: A sample with Au nanodiscs of 100 nm diameter and 30 nm height, a support layer of 7 nm Al_2O_3 and 6 Å Pt was subjected to several temperature ramps. The figure depicts the first and the four last measurements as the sample was found to need a few ramps to find a stable value. Both reactor and sample temperature is included for reference. A clear enhancement of the reaction rate due to illumination is present.

5.2.2 Temperature Ramps

In order to determine the potential effects of the Au nanoantennas, a set of temperature ramps was performed. The reactor temperature was set to increase from 40 °C to 320 °C with 1 °C/min. This corresponds to an increase of the sample temperature from about 30 °C to about 220 °C as measured by the thermocouple. The same sample was subjected to several consecutive temperature ramps both with and without illumination. The samples were found to need a few ramps in order to reach stable values. The results can be seen in Figure 5.7.

Similar measurements were performed on a control sample, containing a support layer of 7 nm Al_2O_3 and 6 Å Pt, but no Au nanodics. Both sample were evaporated at the same time to ensure identical layer thickness. The first two ramps followed the measurements on the sample containing Au nanoantennas closely (Figure 5.8). Multiple measurements were performed under illumination. The results can be seen in Figure 5.9. Although the measurements for the sample without nanoantennas are consistently lower than for those with, no conclusions about possible enhancement from the nanoantennas is drawn at this point.

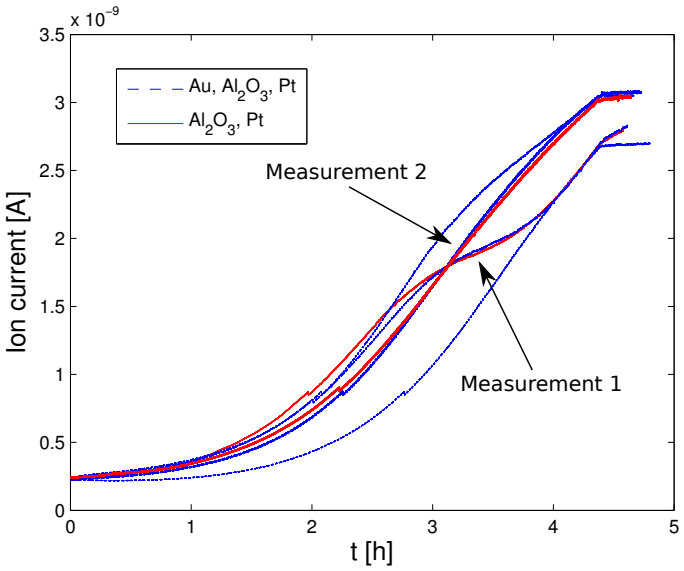

Figure 5.8: A sample with a support layer of 7 nm Al_2O_3 and 6 Å Pt was subjected to several temperature ramps. The figure depicts the first and the second measurements together with the measurements for the samples with Au nanoantennas. The evolving behaviour during the first ramps are very similar between the two samples.

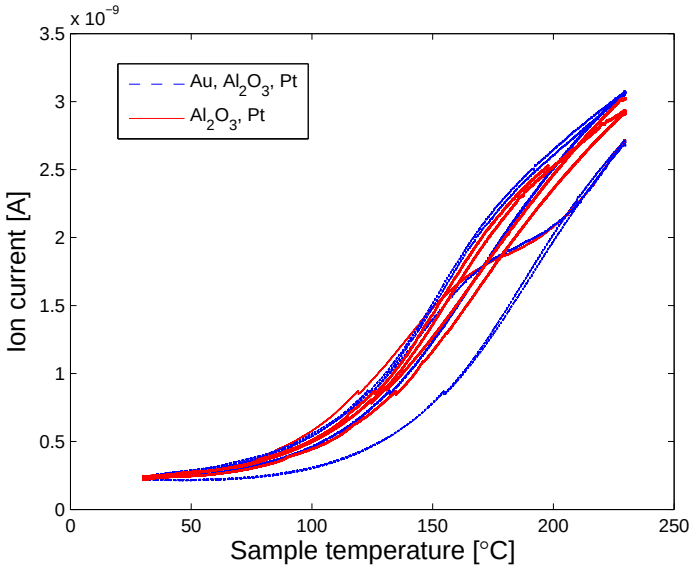

Figure 5.9: The complete set of temperature ramps for both a sample containg Au nanoantennas and a control sample without. From these results, no conclusions about any possible enhancement from the nanoantennas is drawn.

6

Discussion

As the previous chapter demonstrated, the light most definitely has an effect on the reaction. The question being, what light-induced physical phenomenon is responsible for the reaction rate increase?

6.1 Temperature Dependence

Since the reaction rate is highly dependent on temperature, the first candidate is that the light simply causes an increase in temperature. Either on a global scale, where the photons gets absorbed by the material thermalises, or on a more local scale, where the field enhancement due to the nanoparticles induce a local temperature variation. For determining if global temperature increases is the cause of the enhanced reaction rate, a thermocouple was installed in contact with the sample surface. Temperature measurements at different T_R set points show a significant increase in temperature at the thermocouple mounted in contact with the sample surface (Figure 6.1). Similar behaviour of the temperature measured at the thermocouple is found when the same type of measurement is performed, without a sample in the reactor. Hence, this increase is argued to arise from the light heating the thermocouple itself. The actual heating of the sample due to the illumination is argued to correspond to the gradual heating over a longer period of time, that is the difference in temperature increase measured by the thermocouple and the initial offset occurring during the first few seconds. This increase is much more similar to the increase in temperature in the reactor chamber itself. This gradual temperature increase upon illumination is solely present at low T_R set point. For higher reactor temperature, a part of the heat needed from the feedback loop to avoid a temperature decrease due to higher temperature gradients to the surroundings of the reactor is provided by the light. Hence, the

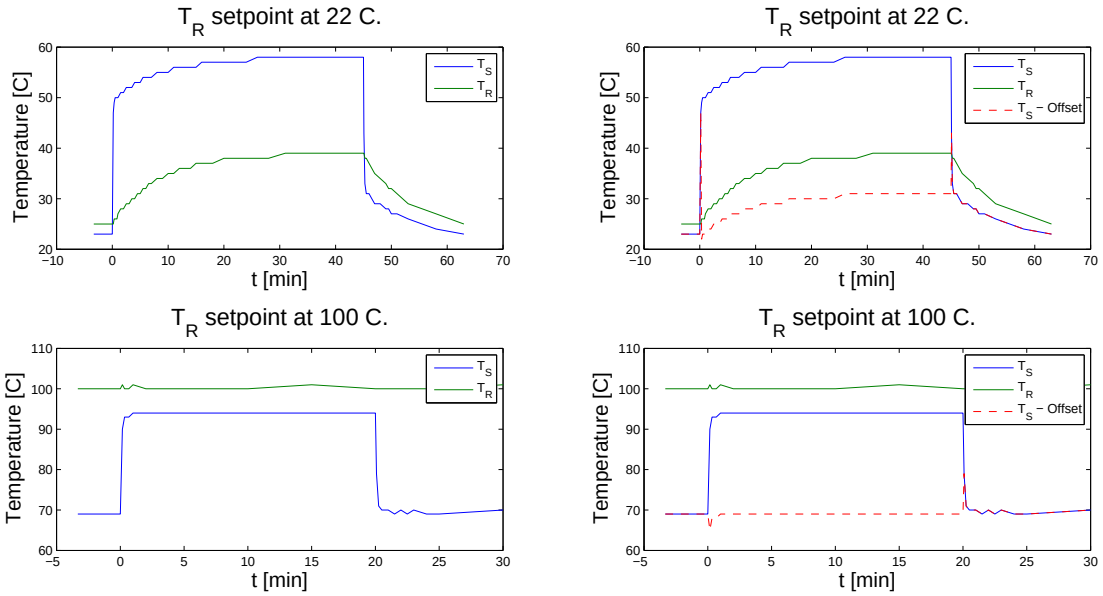

Figure 6.1: Reactor temperature, T_R, and sample temperature, T_S. The temperatures were measured at two different, fix, set-points (22 °C and 100 °C). The light was turned on at $t = 0$. The distinct increase in temperature during the first seconds is presumed to be an effect of the light heating the thermocouple itself. At low temperature, the light has a heating effect on both sample and reactor, this increase in temperature is not present at high temperature set-points.

light does not yield a net temperature change, it aids in keeping the reactor at a higher temperature set point. From this, it is assumed that global temperature increases due to illumination is not the reason for the higher reaction rate during an illuminated temperature ramp.

There is, however, also the question of the limitations of the thermocouple. It only measures the temperature at one part of the sample, and an estimation of the general temperature distribution over the entire sample is hard to come by. A few degrees difference do not explain the large difference between illuminated and unilluminated samples.

On the local scale, Zhdanov et al. performed theoretical studies of a similar systems. Their conclusion was that illumination with 100 W/m^2 would not cause temperature increases of more than a few degrees.[16] It is speculated, that although there are differences between their studied system and the experimental set up, the local temperature differences should not exceed a few degrees.

6.1.1 Step Responce

From the results of the step time measurements, Figures 5.4 and 5.5, conclusions about inherent properties of the experimental set up can be drawn. As one can see from the results, the step response are shaped as one would expect from a convective property from a source. However, it appears separate from the mass flow properties, unaltered by the increase in mass flow. It stands to reason that the step time primarily arises from diffusion through the capillary tube of the mass spectrometer. Increasing temperature do, however, appear to decrease the step time. There might be several factors for this. Visible from the temperature ramps is that at intermediate temperatures ($T_S \in [100,250]\,^\circ C$), the first derivative is higher than at low temperatures, leading to a larger response in production rate to a small increase in heat. Also, at higher temperatures, the kinetics of the system will also be faster, allowing for faster diffusion processes.

The diffusion to the capillary is a short distance in comparison to the distance the gas has to travel through the capillary. Hence, one of the disadvantages with using a mass spectrometer is the loss of kinetic responses.

6.1.2 H Poisoning

The somewhat high temperature needed to sustain a high reaction rate, or rather initiate a higher rate, might depend on that at the given concentrations, $[H_2]=[O_2]$, the surface is likely covered in H as it has a higher sticking coefficient than O. At these conditions, the surface is poisoned by H and a higher temperature is needed to desorb H from the surface, leaving active sites for the O_2 where it can dissociate and react with the H.

6.2 Light Enhancement

Due to the large differences between illuminated and unilluminated samples, and the results from temperature measurements, the reaction increase is presumed to be (at least partly) an effect induced by photons. As the control samples without nanoantennas also display this enhancement, clearly there is an effect in the catalytic particles themselves. At this realisation, a new question arises, do the light induce any effect in the nanoantennas?

As the surface coverage of Au nanoantennas is only partial, about 10%, the bulk of the catalytic particles on the surface do not feel the influence of the enhanced electric field from the antenna. From the results on the control sample, it is clear that the light induces an effect directly in the catalytic particles, it would be plausible that this effect dominates the effect from the Au nanoantennas as only a small part of the catalytic particles would be sensitive to this effect whilst the major part would be subjected to the light induced effect directly in the catalytic

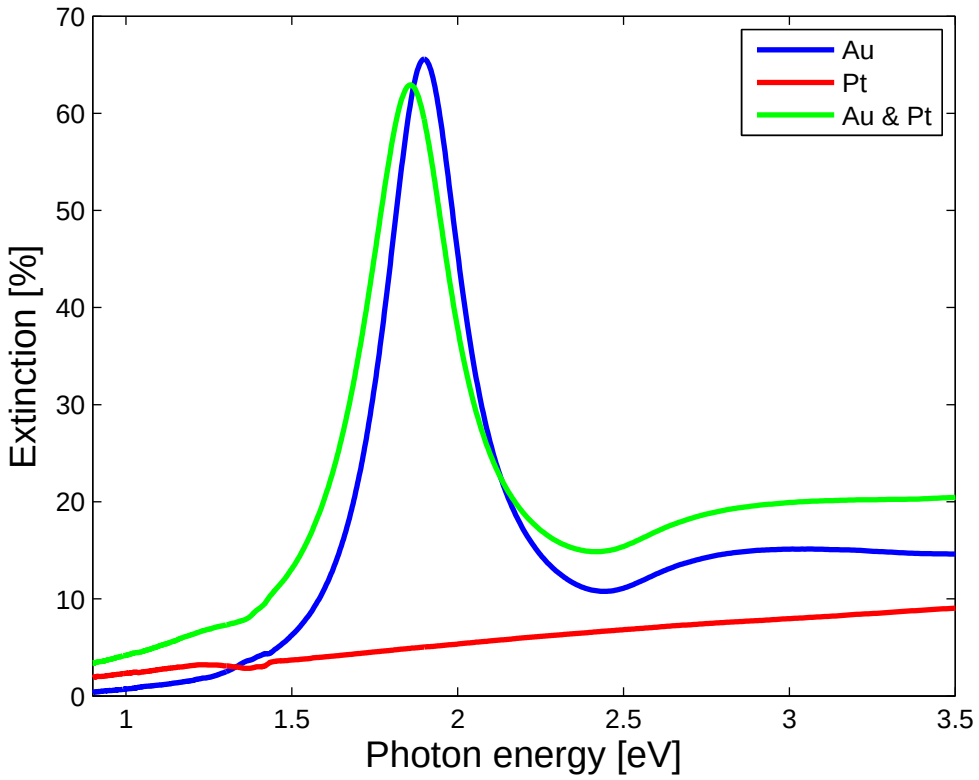

Figure 6.2: The graph contains the extinction spectrum for samples containing only Au nanodsic and only evaporated Pt respectively as well as the extinction spectrum for a sample with both Au and Pt. As the catalytic Pt particles are only a few nanometers, their absorption is primarily in the UV spectral range.[17] Note that the extinction for the sample with both Au and Pt is not the sum of the other two extinction spectra, the resonance peak for the Au disc is altered by the presence of the Pt.

particles themselves. The relative small fraction of catalytic particles subjected to the influence of the antennas might not be visible over the larger fraction responding directly to the incoming photon flux.

For the radiation induced effect in the Pt particles, there are a few different possible reasons. One possible reason is that since Pt also, to some extent, is plasmonically active, the enhanced reaction rate is a result of deexcitation of a plasmonic resonance and a consecutive hot electron transfer. The extinction spectra of the samples were measured, both for samples containing only Au antennas, only Pt particles as well as sample containing both, the resulting spectra can be seen in Figure 6.2. Pt particles of this size do not exhibit a clear peak in the extinction spectrum, they exhibit a broad absorption with centre of mass in the UV spectral range. The extinction is however dominated by absorption for small

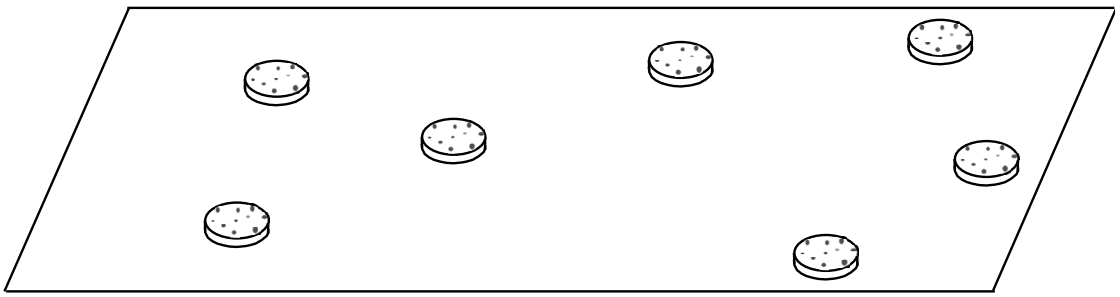

Figure 6.3: Proposed sample for future experiment. Nanoantennas covered in a support layer and Pt catalyst particles. All catalytic particles are in the surroundings of a nanoantenna and should experience the enhanced electric field.

particles.[17]

The other candidate for the enhance reaction rate is direct photoexcitation of hot electrons in the Pt particles. A similar effect was observed by Ljungström et al. in 2001.[18] In their experiment, the oxidation of CO over a Pt or Pd catalyst was measured. A similar reaction enhancement was found and ascribed to photon induced hot electrons in the small catalytic particles which in turn active a surface species.

Excitation of electrons in the support layer is assumed to be negligible due to the large band gap of Al_2O_3.

6.3 Future Prospects

In order to isolate the effect of the nanoantennas, samples where the Pt catalyst has been evaporated on top of the nanoantennas before the hole-mask has been disposed is proposed. In this manner, all the catalytic particles present on the sample will experience the effect of the nanoantennas. Control sample without the antennas should also be measured, from this, the effect of the nanoantennas should be isolated.

From the extinction spectra in Figure 6.2, it is reasonable to assume that the resonance peak of the nanoantennas is at a slightly to low energy. The energy difference of the LUMO of O_2 adsorbed to a Pt(211) surface and the Pt Fermi level is about 2.5 eV.[19] Hence, it would be preferably for dissociation if the resonance peak of the nanoantenna was centred around this energy. Variation of plasmonic metal and particle size can be used to tailor the resonance peak position to match the energy difference of the LUMO of the adsorbed O_2 and the Pt Fermi level.

Another experiment to be tested is a layered sandwich structure. Wadell et al. have created such structures and found that the top layer metal couples to the bottom layer metal.[20]

To establish the light dependence compared to a thermal effect, any wavelength

dependence should be established. This could be accomplished via the use of band-pass filters, by illuminating the sample with one wavelength at a time. If the reaction rate under illumination displays a clear wavelength dependence, the photons themselves are responsible for some of the enhancement.

7

Conclusion

The project concludes that there might be an enhancing effect from the Au nanoantennas, but this needs further study. It also concludes that there is a light induced enhancement of the reaction rate directly in the catalytic particles. With further studies, determination of the possible enhancement from the nanoantennas should be achievable. The cause of the measured reaction enhancement due to the illumination of the Pt particles is not established, but is speculated to be a combination of direct photexcitation and deexcitation of plasmons.

Bibliography

[1] P. Christopher, H. Xin, S. Linic, Visible-light-enhanced catalytic oxidation reactions on plasmonic silver nanostructures, Nature Chemistry 3 (6) (2011) 467–472.

[2] A. Marimuthu, J. Zhang, S. Linic, Tuning selectivity in propylene epoxidation by plasmon mediated photo-switching of cu oxidation state, Science 339 (6127) (2013) 1590–3.

[3] S. Mukherjee, F. Libisch, N. Large, O. Neumann, L. V. Brown, J. Cheng, J. B. Lassiter, E. A. Carter, P. Nordlander, N. J. Halas, Hot electrons do the impossible: plasmon-induced dissociation of h2 on au, Nano Lett 13 (1) (2013) 240–7.

[4] S. Linic, P. Christopher, D. B. Ingram, Plasmonic-metal nanostructures for efficient conversion of solar to chemical energy, Nature materials 10 (12) (2011) 911–921.

[5] K. L. Kelly, E. Coronado, L. L. Zhao, G. C. Schatz, The optical properties of metal nanoparticles: the influence of size, shape, and dielectric environment, The Journal of Physical Chemistry B 107 (3) (2003) 668–677.

[6] C. F. Bohren, D. R. Huffman, Absorption and scattering of light by small particles, Wiley-VCH, 2008.

[7] T. J. Antosiewicz, S. P. Apell, C. Wadell, C. Langhammer, Absorption enhancement in lossy transition metal elements of plasmonic nanosandwiches, The Journal of Physical Chemistry C 116 (38) (2012) 20522–20529.

[8] M. I. Stockman, Nanoplasmonics: past, present, and glimpse into future, Optics express 19 (22) (2011) 22029–22106.

[9] N. W. Ashcroft, N. D. Mermin, Solid state phys, Saunders, Philadelphia.

[10] C. Kittel, P. McEuen, Introduction to solid state physics, Vol. 8, Wiley New York, 1986.

[11] J. D. Jackson, Classical electrodynamics, Classical Electrodynamics, 3rd Edition, by John David Jackson, pp. 832. ISBN 0-471-30932-X. Wiley-VCH, July 1998. 1.

[12] M. I. Stockman, Nanoplasmonics: The physics behind the applications, Physics Today 64 (2) (2011) 39–44.

[13] I. Chorkendorff, J. W. Niemantsverdriet, Concepts of modern catalysis and kinetics, WILEY-VCH, 2006.

[14] R. M. Martin, Electronic structure: basic theory and practical methods, Cambridge university press, 2004.

[15] H. Fredriksson, Y. Alaverdyan, A. Dmitriev, C. Langhammer, D. S. Sutherland, M. Zäch, B. Kasemo, Hole–mask colloidal lithography, Advanced Materials 19 (23) (2007) 4297–4302.

[16] V. P. Zhdanov, I. Zorić, B. Kasemo, Plasmonics: Heat transfer between metal nanoparticles and supporting nanolayers, Physica E: Low-dimensional Systems and Nanostructures 46 (0) (2012) 113–118.

[17] C. Langhammer, B. Kasemo, I. Zoric, Absorption and scattering of light by pt, pd, ag, and au nanodisks: absolute cross sections and branching ratios, J Chem Phys 126 (19) (2007) 194702.

[18] S. Ljungström, D. Chakarov, J. Bergeld, S. Johansson, B. Kasemo, Photoassisted processes for improved catalytic activity and selectivity of environmentally harmful emissions, Topics in Catalysis 16-17 (1-4) (2001) 433–436.

[19] A. W. E. Chan, R. Hoffmann, W. Ho, Theoretical aspects of photoinitiated chemisorption, dissociation, and desorption of oxygen on platinum(111), Langmuir 8 (4) (1992) 1111–1119.

[20] C. Wadell, T. J. Antosiewicz, C. Langhammer, Optical absorption engineering in stacked plasmonic au-sio(2)-pd nanoantennas, Nano Lett 12 (9) (2012) 4784–90.